Journal of Power Sources 435 (2019) 126514

Contents lists available at ScienceDirect

Journal of Power Sources

journal homepage: www.elsevier.com/locate/jpowsour

Electrochemical and microbiological characterization of single carbon granules in a multi-anode microbial fuel cell

Leire Caizán-Juanarena[a,b], Ivonne Servin-Balderas[a], Xuan Chen[a], Cees J.N. Buisman[a,b], Annemiek ter Heijne[a,*,1]

[a] Department of Environmental Technology, Wageningen University, Bornse Weilanden 9, 6708 WG, Wageningen, the Netherlands
[b] Wetsus, European Centre of Excellence for Sustainable Water Technology, Oostergoweg 9, 8911 MA, Leeuwarden, the Netherlands

HIGHLIGHTS

- Carbon granules were tested as bioanodes in multi-anode Microbial Fuel Cells.
- Results were reproducible and statistically reliable.
- Biofilm growth relates linearly to the outer surface area of carbon granules.
- Small activated carbon granules obtain higher volumetric current.
- A large granular specific surface area benefits volumetric charge storage.

GRAPHICAL ABSTRACT

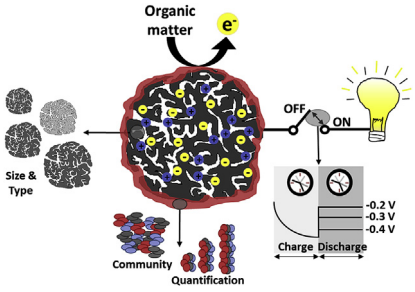

ARTICLE INFO

Keywords:
Capacitive bioanode
Granular activated carbon
Total nitrogen
Microbial community
Charge/discharge cycles
Charge storage

ABSTRACT

Capacitive microbial fuel cells (MFCs) use bacteria on a capacitive anode to oxidize organics in wastewater and simultaneously charge the electrode. This study aims to gain knowledge on the performance of single activated carbon (AC) granules, which are used as capacitive bioanodes. To this end, a multi-anode MFC that allows the testing of up to 29 granules under the same experimental conditions is used. 2 types of AC granules (PK and GAC) and 3 different size-ranges (n = 8 each) are studied in terms of current production, biomass quantification, microbial community and charge storage. Additionally, charge storage of PK granules (n = 24) is determined for different charging/discharging times. Results show that total produced charge directly relates to biomass amount, which has a linear relation towards granule outer surface area. Small AC granules have higher volumetric current densities, which could be of interest for their application in up-scaled reactors. PK granules show slightly higher biomass and current production than GAC granules, while these latter ones show larger volumetric charge storage capacity. Similarly, it is shown that short charging/discharging times are needed to obtain maximum charge storage and current output. These findings are of importance to design and operate MFCs with capacitive properties.

* Corresponding author. Department of Environmental Technology, Wageningen University, Bornse Weilanden 9, Axis-Z (building 118), room 1.102, 6708 WG, Wageningen, the Netherlands.
E-mail address: annemiek.terheijne@wur.nl (A. ter Heijne).
[1] Postal address: P.O. Box 17, 6700 AA, Wageningen [t] +31 317 483447.

https://doi.org/10.1016/j.jpowsour.2019.04.042
Received 13 December 2018; Received in revised form 14 March 2019; Accepted 9 April 2019
Available online 23 May 2019
0378-7753/ © 2019 The Authors. Published by Elsevier B.V. This is an open access article under the CC BY license (http://creativecommons.org/licenses/by-nc-nd/4.0/).

1. Introduction

A microbial fuel cell (MFC) is a bio-electrochemical system that allows for simultaneous degradation of organic matter in wastewater and production of electricity by the use of microorganisms, also known as electrochemically active bacteria (EAB) [1,2]. Compared to the conventional wastewater treatment process, MFCs can recover chemical energy from wastewater that has low concentration of organics [3], without demanding energy for aeration [4] and reducing sludge production [5]. Thus, it can be considered a promising and cost-efficient technology for wastewater treatment [6–8]. However, the recently reported power production by most MFCs can only reach up to 2–3 $W\,m^{-2}$ [9], which is still relatively low compared to anaerobic digestion. How to increase the power output is still a remaining challenge and so there are many research studies focused on that domain [10–13]. One possibility is to combine MFCs with capacitors, which act as an energy storage system to improve the power output [14,15]. Dewan et al. [16] used an external capacitor to collect the generated power by an MFC and dispensed it intermittently, which showed an advantage in providing energy for high-power-consuming devices. It is also possible to integrate a capacitor within the MFC by the use of capacitive materials as electrode [17,18]. Deeke et al. [19] tested an internal capacitor by using a graphite plate coated with activated carbon powder and a polymer solution, which outperformed a non-capacitive electrode in terms of current density and charge recovery.

The electrode material on the anode plays a vital role in MFCs, as it is the place where the biofilm attaches and electron transfer takes place [5,20]. By optimizing anode properties such as surface area or roughness, among others, electron transfer can be enhanced and thus the overall MFC performance can be improved [21]. Carbonaceous materials are the most widely used materials for bioanodes, as they have good biocompatibility, good chemical stability, high electrical conductivity and relatively low cost [22,23]. Carbon materials with three-dimensional structure and high surface-area-to-volume ratio are of special interest, as they can increase volumetric power outputs [24,25]. Activated carbon (AC) granules have a very porous structure that provides them with a large specific surface area (SSA > 1000 $m^2\,g^{-1}$) [26], which benefits the amount of catalytic sites (and thus the number of electron transfer) but also allows charge storage [27]. This feature is particularly important in MFCs with an internal capacitor, where the electrons produced by EAB (i.e. faradaic current) are stored in the form of electrochemical double-layer (EDL) [28–30]. The electrochemical double-layer (EDL) is a known charging mechanism of the so-called electrochemical double-layer capacitors (EDLCs) [31,32], which confers features (e.g. energy density, power density, charge/discharge cycle lifetime) intermediate between batteries and conventional capacitors by the use of carbon porous electrodes such as activated carbon or carbon nanotubes [33–36]. In MFC studies with an increased capacitance of the electrodes, the overall performance of the cell was boosted due to an increase of microbial attachment to the electrode, total produced charge and current and power densities [37–39]. Particularly AC granules have been used in different reactor types as electrodes, where they are mobilized by stirring [40], fluidization [41–46] or both fluidization and recirculation [9], thus intermittently contacting the current collector.

The intermittent contact of AC granules with the current collector in fluidized bed reactors benefits from the capacitive properties of AC granules, as the current produced by EAB can be stored in the granule during the *Off* period (no contact with the current collector) and be released at a later stage during the *On* period (in contact with the current collector). Fluidized bed reactors have several advantages compared to classical MFCs, such as the reduction of clogging and ohmic losses, the use of less electrode and membrane materials, and a better competition of electrogens over methanogens [47]. To reach reasonable current densities in such reactors, it is crucial to improve the biofilm growth on granules but also the contact between granules and current collector. To assess the maximum performance of AC granules in such a system, Borsje et al. [48] studied the electrochemical performance of single AC granules as bioanodes. The produced current density reached up to 76 and 63 $mA\,cm^{-3}$ at −0.3 V for AC granules commercially known as PK and GAC, respectively, which is several orders of magnitude higher than the currents obtained in fluidized reactor systems [9]. The potential of single AC granules was thus demonstrated, as well as the possibility to provide valuable information for optimizing up-scaled systems that use this material. However, it is needed to build further on these findings by the study of e.g. more granules that can show reproducibility, important engineering parameters such as granule size, biofilm growth or charge storage at different intermittent operation conditions, among others.

In this study, a multi-anode MFC was built, which allowed for the growth and monitoring of 24 single AC granules under same conditions. The aim was to test several variables of interest for the use of AC granules in MFCs in a reproducible way, looking into outputs such as current production, charge storage, biofilm growth and microbial community of AC granules. The challenges were to: i) determine the performance of different types and sizes of AC granules; and ii) determine the influence of anode discharging potential and optimum charging/discharging times on charge storage.

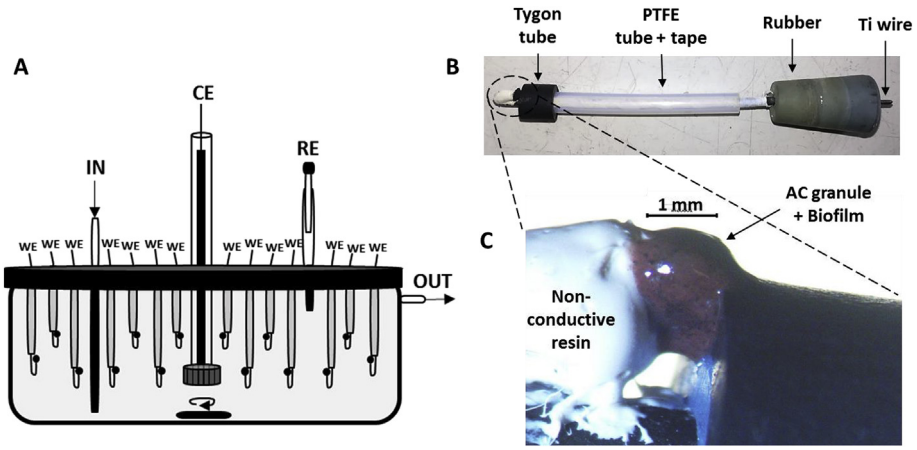

Fig. 1. A) Representation of the custom-made multi-anode MFC. B) Picture of a custom-made clamp to hold a single AC granule. C) Biofilm growth on a single AC granule placed on the tip of a clamp.

2. Materials and methods

2.1. Setup of the multi-anode MFC

The custom-made MFC reactor (Fig. 1A) consisted of two compartments: a 2.3 L container as the anode chamber and a glass tube attached to a funnel as the cathode chamber. The anolyte (10 mM $NaCH_3COO{\cdot}3H_2O$; 1 mL L^{-1} Wolfe's vitamin solution; 1 mL L^{-1} Wolfe's modified mineral solution; 3.7 mM NH_4Cl, 1.7 mM KCl; 30.5 mM $Na_2HPO_4{\cdot}2H_2O$; 19.5 mM KH_2PO_4) consisted of 2 L of which 0.2 L was inoculum from another active MFC run on acetate, leaving a headspace of 0.3 L. The cathode chamber had approximately a volume of 0.13 L (100 mM K_3FeCN_6; 30.5 mM $Na_2HPO_4{\cdot}2H_2O$; 19.5 mM KH_2PO_4) and was placed in the centre of the anode chamber. The cathode was 24 cm^2 of graphite felt attached to a titanium wire (1 mm diameter, 36 cm long) as the current collector. To connect both chambers, a 1.76 cm^2 cation exchange membrane (Fumasep FKB, FuMa-Tech GmbH, St. Ingbert, Germany) was placed on the bottom of the cathode chamber. The lid of the container had one hole for the inflow of substrate, one hole for the reference electrode (Saturated KCl Ag/AgCl) and 29 holes for the working electrodes. Additionally, a hole was made on the side of the container for the outflow. The effect of the distance between working and the reference electrodes on current production was neglected as the latter one was placed outside of the electric field. All potential values in this paper are reported versus Ag/AgCl reference electrode (+0.199 V vs NHE).

Single granules were held up separately with custom-made hook-shaped clamps (Fig. 1B). The core of the clamps was titanium (Ti) wire (1 mm diameter) covered by a heat shrink tube (RS Pro 389–634) to prevent its oxidation and the growth of biofilm on its conductive surface. The clamp was passed through a PTFE tube (Polyfluor Plastics BV) surrounded by Tygon® tube (Saint-Gobain Performance Plastics) on the tip. PTFE tape was placed between the PTFE tube and the Ti wire in order to create resistance and ensure a proper and enduring contact with the granule. On the tip of the clamp, a layer of conductive glue (EMS, Pennsylvania, USA) was added and its contact area with the granule was minimized with non-conductive resin (Revlon® Colorstay™) to limit bacterial growth on the clamp. The other side of the titanium wire was passed through a rubber that fitted on the holes made for the working electrodes. The average resistance of the clamps was 0.8–1 Ω between the two ends. Each clamp was connected to a channel from the MultiWE32 module (Ivium Technologies, Eindhoven, the Netherlands). This module can operate up to 32 working electrodes that share a common reference electrode and counter electrode. All channels can be simultaneously controlled and sampled with restricted operation modes. Fig. 1C is an example of an AC granule in a clamp with the biofilm in red.

2.2. Carbon granules

All the granules were first sieved (aperture sizes 2, 2.8 and 4 mm, Retsch®, Germany) and then individually selected for an approximate spherical shape and weighted (Mettler Toledo, d = 0.001 mg). Table 1 contains the exact size range and weight information about each of the granules used in this study. After selection, granules were treated with 22% hydrochloric acid (HCl) for 24 h and washed 3 times with demi water [49]. This is a common practice to remove surface organic contamination and metal impurities and thus standardize the electrode material under study for comparative purposes.

To analyse the influence of the electrode material and size, two types of activated carbon with the commercial names of PK 1–3 and GAC 830W (Cabot Norit Nederland B.V., Amersfoort, the Netherlands) and three ranges of sizes for PK granules (small, 1.0–2.0 mm; medium, 2.0–2.8 mm; large, 2.8-4.0 mm) were tested in the same reactor. Altogether, 24 granules were tested: 6 GAC small granules, 6 PK small granules, 6 PK medium granules and 6 PK large granules. Same granules for the small size-range were used to analyse the influence of the discharging anode potential on charge storage. A new reactor was built with 24 PK granules of three size ranges, 8 granules of each. Only the small granules were used to study the effect of different charging/discharging times. As control, three glass beads (B Braun biotech international, Schwarzenberg, Germany) of 2 mm diameter covered with PTFE tape were clamped and placed in each reactor. For scanning electron microscopy (SEM) and next-generation sequencing (NGS) experiments, graphite granules (GG), i.e. non-activated carbon granules, were also placed in the reactor.

Table 1
Weight and size distribution of the granules selected for the study of: i) granule size, type and potential ii) scanning electron microscopy (SEM) images, iii) next-generation sequencing (NGS) analysis and iv) charging/discharging times.

	Carbon granule	Small (1.0–2.0 mm)	Medium (2.0–2.8 mm)	Large (2.8–4.0 mm)
Size & Type & Potential	PK 1-3	1.5–2.0 mg	3.2–3.9 mg	7.5–9.7 mg
	GAC 830W	1.8–2.3 mg	–	–
SEM images	PK 1-3	–	4.2–6.0 mg	8.1–10.3 mg
	GAC 830W	–	7.6–9.4 mg	11.2–29.8 mg
	GG	–	18.2–22.1 mg	46.2–50.8 mg
NGS analysis	PK 1-3	–	3.9–6.1 mg	–
	GAC 830W	–	4.5–7.0 mg	–
	GG	–	8.6–14.2 mg	–
Charging/ Discharging times	PK 1-3	1.8–3.0 mg	5.0–8.9 mg	10.0–23.3 mg

The weight of the granules was the only parameter that was measured, while the size was ensured within certain ranges. Therefore, the volume of the granules was estimated by using the apparent density values from the manufacturer: 0.3 g mL^{-1} for PK granules and 0.5 g mL^{-1} for GAC. These are different densities from those used in a previous study for the same type of granules [48]. To estimate the outer surface area (SA) from the granule volume, a spherical granule was assumed, without considering the possible roughness or pores where bacteria could have access to. As for the specific surface area (SSA), values from a previous study (764 $m^2 g^{-1}$ for PK granules and 885 $m^2 g^{-1}$ for GAC granules) [48] were used, measured for a pore width range of 0.3–50 nm. These values were the result from applying a model (2D-NLDFT) to N_2 adsorption measurement data.

2.3. MFC operation

Right after granules were placed in the reactor, cyclic voltammetry (CV) scans (3 cycles, −0.3 V to −0.48 V, at a scan rate of 0.3 mV s^{-1}) were performed to verify if the cables of the MultiWE32 module worked well and if the contact between granule and clamp was good (see Supporting Information, chapter S1). After, granules started to be controlled at a constant anode potential of −0.35 V and current was monitored during one week. Batch mode was maintained for approximately 3 days after inoculation in order to prevent the wash out of inoculum. Continuous mode was then started by pumping anolyte at a rate of 200 μL min^{-1}, which translated in an HRT of 7 days. 3 solutions (acetate, PBS with mineral and vitamins, and demi-water) were placed in separate bottles in the fridge (at 4 °C) and were continuously flushed with N_2 gas to keep them anaerobic. The pump (Gynkotek M480 CS HPLC Pump - High Precision Pump) was able to mix the solutions, at a ratio of 1:1:2, to have the desired final concentration. The catholyte was replaced once its colour faded (pointing out complete reduction of K_3FeCN_6). In addition, an oxygen sensor spot (PreSens- Precision Sensing GmbH, Regensburg, Germany) was used to monitor the oxygen level in the anolyte, which was kept below 0.1% (= 0.036 mg L^{-1}). A magnetic stirrer at 100 rpm was used to minimize mass transfer

limitations and temperature was controlled at 30 °C. Samples (2 mL) were taken daily from the anolyte to measure pH, and stored after at −80 °C for further acetate analysis. Current was recorded every 600 s.

In the study concerning the type and size of granules as well as the applied anode potential, about 7 days after inoculation clamps were disconnected and granules were collected. Just before that, 3 charge/discharge cycles of 600 s each were done. Charge was done at open circuit (OC) and discharge at a constant potential of −0.2 V, −0.3 V or −0.4 V. Only because granules were placed in the same reactor we were able to compare between them. Same was done for SEM images, where 8 granules (4 medium and 4 large) of activated (PK and GAC) and non-activated carbon granules (GG) were placed in the same reactor and controlled at −0.35 V for 9 days (see Supporting Information for cumulative charge, chapter S2). For NGS analysis, same procedure was followed but for 5 granules of each type and for 15 days to ensure enough bacterial growth (see Supporting Information for cumulative charge, chapter S3). As for the study of charging/discharging times, growth was maintained up to 3 weeks in which charge/discharge cycles were done regularly (every 2–3 days) as previously explained. Before collecting the granules, different charging and discharging time combinations were applied with 2, 5, 10 and 15 min at −0.2 V and −0.3 V as discharging potentials. Combinations between 2 and 15 min were not addressed, and the discharging potential of −0.4 V was not contemplated as little charge could be measured. The faradaic current, i.e. the current produced from acetate oxidation, was determined from the steady-state current recorded after 600 s of stabilization period during discharge. This current was used to calculate the capacitive current, i.e. the current released from the EDL formation, according to Eq. (1).

$$Q_{Stored} = \int_0^t I_C \, dt = \int_0^t (I_T - I_F) \, dt \quad (1)$$

; where Q_{Stored} is the stored/capacitive charge (C), I_C is the capacitive current (A), I_F is the faradaic current (A) and I_T is the total current (A) as result of the sum up of capacitive and faradaic currents. More information on current and potential behaviour of capacitive electrodes can be found in previous research [19,48].

2.4. Total nitrogen (TN) analysis

Total nitrogen (organically and inorganically bounded) was determined as indication of the amount of biomass attached to AC granules. After one week of bacterial growth, granular bioanodes were collected from the reactor and biofilm growth was quantified (as total nitrogen). They were first washed in a buffer solution without NH_4Cl to avoid measuring nitrogen from the anolyte. After, granules were processed according to the protocol of Laton Total Nitrogen cuvette test 20–100 mg L^{-1} TN_b (LCK 338, HACH®, Dusseldorf, Germany). Note that the kit works in terms of volume, therefore 0.2 mL of miliQ water was added in the reaction vessel together with each AC granule. After other chemicals were added, the digestion step consisted of 30 min at 120 °C. 0.5 mL of the final sample was transferred from the reaction vessel to the LCK cuvette, from which the nitrogen concentration was read. Some (PK) granules were again checked for nitrogen content after the first TN analysis to verify if any biomass was left behind. Nitrogen content of those granules was 1.9 ± 0.4 μg N (average of 3). Similarly, clean (PK) granules without biomass but with the same acid treatment were also measured for TN as control. Nitrogen content of those granules was 1.3 ± 0.1 μg N (average of 3). These TN contents are more than 5-fold lower than those measured for the smallest PK granules (see next section).

2.5. Acetate quantification

Liquid samples taken from the reactor were centrifuged for 10 min at 10000 rpm to remove the biomass. Part of the supernatant was mixed with formic acid (15%) in a 9:1 ratio and added to the GC vessels that were well closed with rubber lids. Acetate concentration was analysed with the gas chromatograph (Agilent 7890B). Split injection (1:25, 1 μL volume) was done at constant temperature (250 °C) in a HP-FFAP column (25 m × 0.32 mm x 0.50 μm) with helium as the carrier gas (grade 5.0, at 2 mL min^{-1} column flow). A flame ionization detector (FID, 240 °C) was used and data were recorded with Chromeleon™ CDS software (6.80 SR13).

2.6. Scanning electron microscopy (SEM) imaging

Granules were individually collected from the reactor and fixated with 2.5% glutaraldehyde for 2 h at room temperature. Afterwards, they were rinsed 3 times with a phosphate buffer solution (30.5 mM Na_2HPO_4 and 19.5 mM KH_2PO_4) and dehydrated with a sequence of ethanol solutions (30%, 50%, 70%, 90% and 100%) for 30 min each. Finally, granules were dried at 105 °C for 1 h. For the imaging, single granules were placed in a specimen holder of the scanning electron microscope (SEM) JEOL JSM-6480 LV (JEOL Technics Ltd., Tokyo, Japan). With a magnification of 30–100,000x, SEM was operated at an acceleration voltage of 3–10 kV and an electron beam diameter of 20–30%. Images were analysed with the software JEOL SEM Control User Interface version 7.07.

2.7. Next-generation sequencing (NGS) analysis

Five granules of each carbon type were harvested, cleaned individually with phosphate buffer and placed in the same Eppendorf for storage at −80 °C. Genomic DNA was extracted with the Powersoil® DNA isolation kit (MO BIO Laboratories, Carlsbad, CA, USA) and used to amplify the V3-V4 region of 16S rDNA according to the standard illumine library preparation method described by Takahashi et al. [50]. The same primer sets were used to analyse both bacteria and archaea. Taxonomic analysis was performed by using the QIIME software (package version 1.9.1) and OTU picking was done by the SILVA 128, 16S reference database and the uclust tool [51]. The same SILVA reference database was subsequently trained by the RDP classifier to perform OTU classification [52].

2.8. Statistical analysis

Differences in current production, total produced charge, nitrogen and charge storage were analysed with one-Way ANOVA at $p < 0.05$ with IBM SPSS Statistics 20, using the following factors: type of activated carbon (PK or GAC), size of activated carbon (small, medium or large) and discharging anode potential (−0.4 V, −0.3 V or −0.2 V). All granules compared with this method were grown under same environmental conditions. The assumption of normality was tested with Shapiro-Wilk statistics and homogeneity of variance was assessed with Levene's test. In case the variance between groups was high or the number of samples between groups was unequal, Welch's *t*-test was performed.

3. Results and discussion

3.1. Current production by different types and sizes of single AC granules under continuous growth conditions

Performance of different granule types and sizes placed in the same reactor was compared. Fig. 2A shows the current produced by each type of granule (with standard deviations) as a result of average values of 6 granules for PK and GAC, and 3 glass beads for controls. Generally, all granules followed the same growth pattern, with a maximum current around 3 days after inoculation and a steady-state current of 65–71% of the maximum current after 1 week of growth. This shape seems to be typical for potential controlled bioanodes as previously reported in

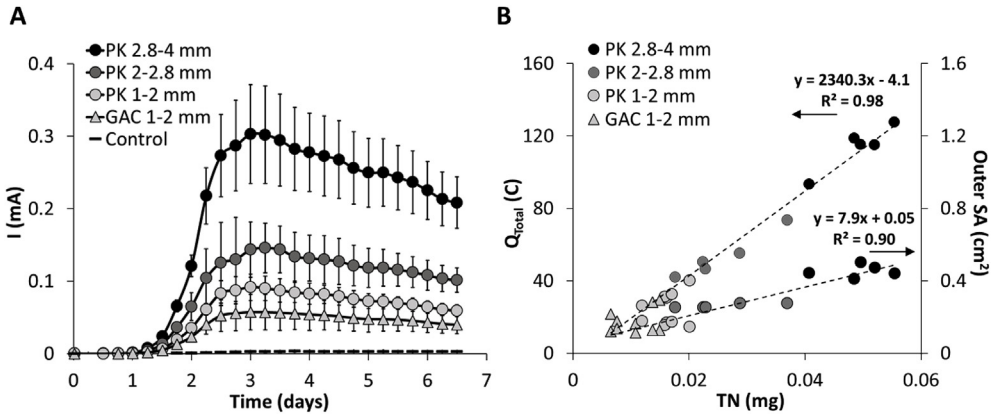

Fig. 2. A) Current production (mA) of three sizes of PK and small GAC granules controlled at a constant potential (−0.35 V vs Ag/AgCl). Each data point represents the average current value of every 0.25 days. B) Total produced charge (C; primary axis) by each granule during the whole growth period and estimated granule outer surface area (cm^2; secondary axis) as a function of total nitrogen (mg).

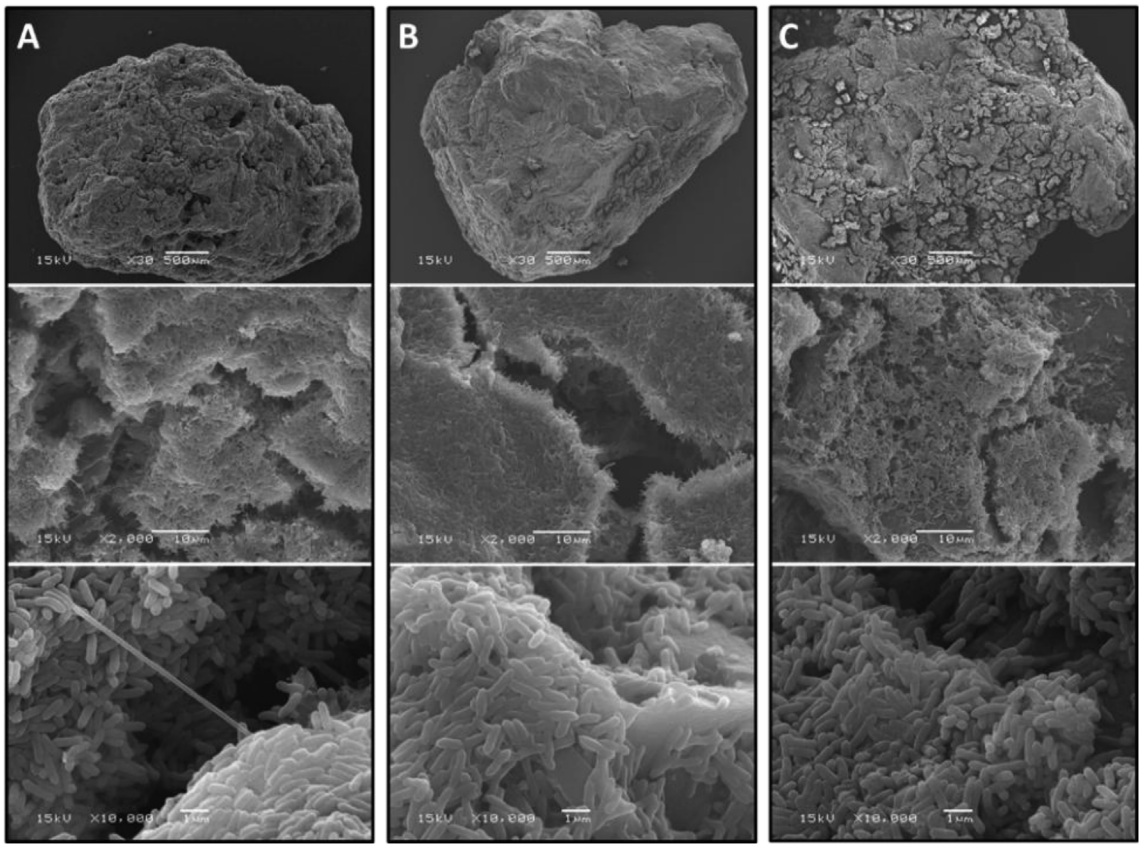

Fig. 3. SEM images of PK (A), GAC (B) and GG (C) granules at different magnifications: ×30 (up), ×2000 (middle) and ×10000 (bottom). For this figure, a medium and a large granule were used for PK (4.4 and 8.1 mg), GAC (9.4 and 29.8 mg) and GG (22.1 and 50.8 mg) granules. They were controlled at −0.35 V vs Ag/AgCl in the same reactor for 9.4 days.

literature [53], which could relate to an increased ionic diffusion resistance due to the formation of a thicker biofilm [54]. Nevertheless, nutrients and substrate were continuously supplied (acetate concentration was maintained > 5 mM) and the solution was continuously stirred (Fig. 2).

Average currents, after the maximum was reached (around 3 days after inoculation), were from high to low: 0.3 ± 0.05 mA for large PK, 0.1 ± 0.03 mA for medium PK, 0.1 ± 0.01 mA for small PK and 0.05 ± 0.02 mA for small GAC granules. However, when normalized to granule weight, small PK granules had the highest current densities, 43.3 mA g^{-1}, followed by medium PK (34.2 mA g^{-1}), large PK (31.7 mA g^{-1}) and small GAC (24.6 mA g^{-1}) granules. These values are in the same range to those previously found for single PK and GAC granules at −0.3 V anode potential, i.e. 58 mA g^{-1} and 24 mA g^{-1}, respectively [48]. The current measured for controls was more than 10 times lower than the current produced by granules, i.e. 0.003 ± 0.001 mA, showing that the contribution of the current collector (clamp) to the current production by single AC granules was negligible.

Total produced charge was calculated as a result of the current produced throughout the whole growth period. Average values were 107 ± 20.4 C for large PK, 51.2 ± 12.2 C for medium PK, 31.4 ± 4.8 C for small PK, and 20.5 ± 7.6 C for small GAC granules. Fig. 2B shows a positive relation between the produced charge and total nitrogen content of each granule, which is expected as both parameters are meant to increase with bacterial growth. The relation found was 2340.3C mg^{-1} N (R^2 = 0.98), which is half of that found for bioanodes in flat (FTO) electrodes, i.e. 4982.2 C mg^{-1} N [53]. The lower value

obtained in this study could relate to a lower microbial activity of the biofilm or to a higher nitrogen content of the same, although it is difficult to say since the bioanodes measured in FTO were grown between 1 and 24 days. Similarly, the graph shows an increased nitrogen content with increased granule size. This was found to be related to the estimated outer SA of granules, which had a linear relation ($R^2 = 0.9$) towards the amount of biomass. In fact, large PK granules had most biomass (0.05 ± 0.005 mg) followed by medium PK (0.03 ± 0.007 mg), small PK (0.02 ± 0.003 mg) and small GAC (0.01 ± 0.004 mg) granules. Differences in current were significant between all PK sizes among each other ($p < 0.05$), meaning that higher currents were related to more biomass on larger granules. Differences between small PK and GAC granules were non-significant in terms of produced charge and total nitrogen ($p = 0.47$ and $p = 0.37$, respectively), probably due to their similar estimated outer SA (0.16 ± 0.01 cm^2 and 0.12 ± 0.01 cm^2 in average, respectively).

3.2. Biofilm visualization and microbial community determination in activated and non-activated carbon granules

Biofilm growth was also assessed by means of SEM images and genetic sequencing for activated (PK and GAC) and non-activated (GG) carbon granules, which were grown in the same reactor and under the same conditions. Fig. 3 shows the surface of granules (see Table 1) at different magnifications after 9.4 days of growth. They were all covered by biofilm with no apparent differences among each other, which could mean that: i) the activation process of carbon granules did not have an influence on bacterial growth; ii) the available surface area where bacteria can grow (> 0.5 μm, bacterial size [55]) is similar in every granule type; iii) the surface roughness of all granules is high enough for the attachment of bacteria or, instead, has no influence after the first layer of bacterial growth; or iv) the operation conditions (e.g. a continuous growth, potential control, good contact of the electrode with the current collector and little shearing forces) led to a well-developed biofilm no matter the electrode material. The average produced cumulative charge by each granule type (4 medium and 4 large granules) in the reactor was 83.3 ± 29.3 C for GG, 56.1 ± 19.7 C for GAC and 53.3 ± 0.5 C for PK granules (see Supporting Information, chapter S2). Based on these data it seems that, under continuous growth, activated carbon granules did not provide any advantage in terms of biofilm growth and current production compared to non-activated carbon granules, which have in contrast very few pores and therefore have low charge storage capacity. These results contradict what was found in a previous study [19], where the increased current densities of flat capacitive electrodes over non-capacitive ones under continuous growth (at −0.4 V vs Ag/AgCl) were attributed to the increased roughness of the former.

Microbial community of the biofilm was characterized for the same type of carbon granules (see Table 1) but in another run that lasted 15 days (see Supporting Information, chapter S3). Fig. 4 shows the composition of the microbial community, which was similar among the three types of granules. *Geobacter* spp. accounted for 50% of the microbial community in PK granules, 31% in GAC granules and 43% in GG granules. The next most abundant microorganisms were within the family of *Rhodocyclaceae*, which accounted for 11–14.3% of the total microorganisms, and the genus *Acetobacteroides* with relative abundances of 6.4–12.1%. Other bacteria (with > 1% of relative abundance) belonging to the phyla of *Proteobacteria*, *Bacteroidetes*, *Firmicutes* or *Synergistetes* could also be found in the biofilm. This is a similar microbial community composition to what was determined in other studies for bioanodes [56]. Some studies have searched for changes in microbial composition and biofilm morphology for different electrode materials (surface functional groups) [56,57] and operation modes (periodic polarization over constant control) [58]. However, in this study, the similar composition and relative abundance of microorganisms as well as current production indicate that the above-mentioned

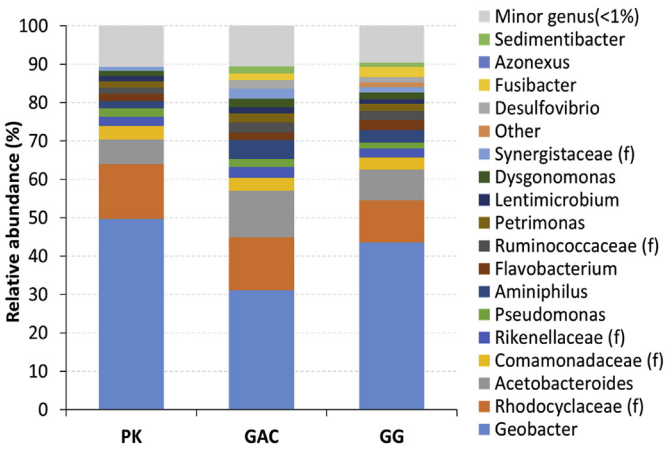

Fig. 4. Microbial community at the genus level of three types of carbon granules: GG, GAC and PK. (f) = family level, as the genus was unknown. Granules were controlled at −0.35 V vs Ag/AgCl in the same reactor for 15 days.

granule properties did not affect biofilm growth or, instead, those properties were overruled by e.g. the continuous and potential controlled operation mode.

3.3. Influence of the anode discharging potential and charging/discharging times on charge storage of PK and GAC granules

Experiments were performed at OC (charging) and potential control (discharging) to study charge storage in PK and GAC granules. Here, we report on the results for small granules. Overall, more positive discharging potentials increased the released charge of PK and GAC granules belonging to the EDL formation process, i.e. charge storage, as shown in Fig. 5. This is expected as, when the potential difference between charging and discharging processes increases, the driving force to harvest electrons also increases, leading to a larger charge storage value. Nevertheless, only −0.2 V obtained significantly different values compared to the other two potentials ($p < 0.01$). PK granules had an average stored charge of 1.4 ± 0.5 mC, 4.5 ± 1.8 mC and 15 ± 4.4 mC at discharging potentials of −0.4 V, −0.3 V and −0.2 V, respectively, while GAC had an average stored charge of 1.8 ± 0.7 mC, 5.5 ± 2.7 mC and 16.2 ± 6.8 mC at same potentials. Even though GAC obtained overall higher values than PK granules (Fig. 5A), when normalized to the calculated specific surface area, PK granules showed higher values (Fig. 5B) meaning their surface area is used more efficiently for charge storage. This could relate to the increased mesoporosity (2–50 nm pore size) of PK granules (40%) compared to that of GAC granules (20%) [48], which has been related in literature to an increased double-layer capacitance [35,59]. The pore size distribution could also be the reason for differences in the discharge behaviour of each granule type; PK granules had 80% of charge recovery (of the total stored charge released in 10 min) after 2 min of discharge, while GAC granules reached the 80% charge recovery after 3 min of discharge (see Supporting Information, chapter S4). This delay in GAC granules could relate to their increased microporosity (< 2 nm pore size) contribution (80%) compared to that of PK granules (60%), which could limit the ion transport [48]. Nevertheless, differences in charge storage between materials were non-significant at every potential with and without normalization ($p = 0.22$–0.82).

As the measurement of charge storage depends on the discharging time (t) used to determine it (see Eq. (1)) and the charging time used by bacteria to produce electrons, we studied the effect of combining different time intervals (2, 5, 10 and 15 min) for OC periods (charge) and constant potentials (discharge) on charge storage. Fig. 6A shows the absolute values of stored charge by small PK granules (see Table 1) for every measured combination at −0.3 V discharging potential. In

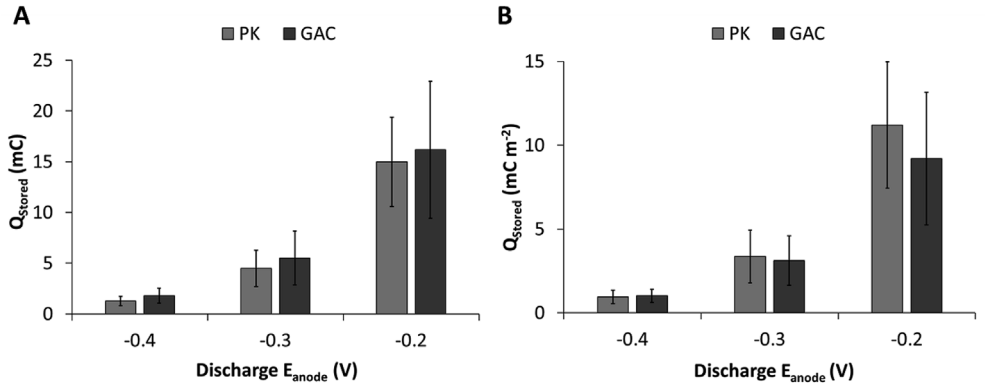

Fig. 5. A) Absolute values of stored charge (mC) and B) stored charge normalized to SSA (mC m^{-2}), both as a function of anode discharging potential (−0.4 V, −0.3 V and −0.2 V vs Ag/AgCl) for small PK and GAC granules 7 days after inoculation.

general, and based on statistical analyses, stored charge 2 min of charge was significantly lower than 10 and 15 min of charge ($p < 0.01$). This was not the case at the shortest discharging time, where 2 min of charge had non-significant differences compared to the rest of charging times. Similarly, no significant differences could be found between 5, 10 and 15 min of charge ($p = 0.3–1.5$). As for discharging times, no significant differences were found among them ($p = 0.1–1$). However, if we look at the total duration of the cycle, shorter charge/discharge cycles might be beneficial not only to increase overall charge storage compared to longer cycles but also to reduce the number (mass) of granules needed in the system. As an example, a cycle of 5-2 min can store 8.7 mC, while in that same time 1.75 cycles of 2-2 min can store 14.5 mC.

If we calculate the total produced charge (faradaic + capacitive), it increased linearly with longer discharging times due to longer faradaic currents. In the case of small PK granules, the total produced charge after 10 min of OC increased from 32.5 ± 5.6 mC with 2 min of discharge to 171.7 ± 19.4 mC at 15 min of discharge. Deeke et al. [19] also studied the effect of different charging/discharging times on the total produced charge and indeed found that longer discharging times favoured total produced charge. However, longer discharging times might not be preferable as it limits the contribution of capacitive current. To get more insight about faradaic and capacitive currents, contribution (%) of stored charge to the total produced charge was calculated (Fig. 6B). If we consider charging times, similar statistical results to those explained for absolute charge storage values were found. On the contrary, shorter discharging times led in general to significantly larger contribution of the capacitive charge to the total charge ($p < 0.02$). Therefore, from the results we conclude that 2 min of discharge should be combined with 2 min of charge for the highest contribution of stored charge to the total produced charge, same as for the highest absolute values previously presented. Similar trends were found for PK granules at −0.2 V, with overall higher absolute values and contributions of charge storage due to a larger driving force (see supporting Information, chapter S5).

It is important to highlight that charge storage was highly variable at different stages of biofilm growth. For example, the same small PK granules (from the charging/discharging times experiments) had a charge storage of 9.3 ± 2.5 mC at day 4, 18.8 ± 2.5 mC at day 7, and 16.2 ± 2.5 mC at day 10 (discharging potential = −0.3 V vs Ag/AgCl). This makes sense if we consider that EDL formation will largely depend on bacterial activity at OC conditions. Therefore, it is important to always compare the performance of bioanodes that have strictly grown under the same conditions and for the same amount of time if any conclusion on the electrode material wants to be withdrawn, as done in this study.

3.4. Outlook

As shown in the results section, the outer SA of granules plays an important role in current production, with larger granules providing larger SA for bacterial growth. However, from an engineering point of view, volumetric current densities are most important, as the amount of granular electrode material needed for a system will be generally evaluated per volume. The highest volumetric current densities (average values after the maximum was reached) were achieved by small PK and GAC granules, 12.4 ± 1.7 mA mL^{-1} and 12.2 ± 1.4 mA mL^{-1}, respectively, followed by medium (9.9 ± 1.1 mA mL^{-1}) and large (9.1 ± 1.0 mA mL^{-1}) PK granules. However, no significant differences were found between them ($p = 1.4–1.5$). Additionally, the surface-area-to-volume ratio (SA:V) of

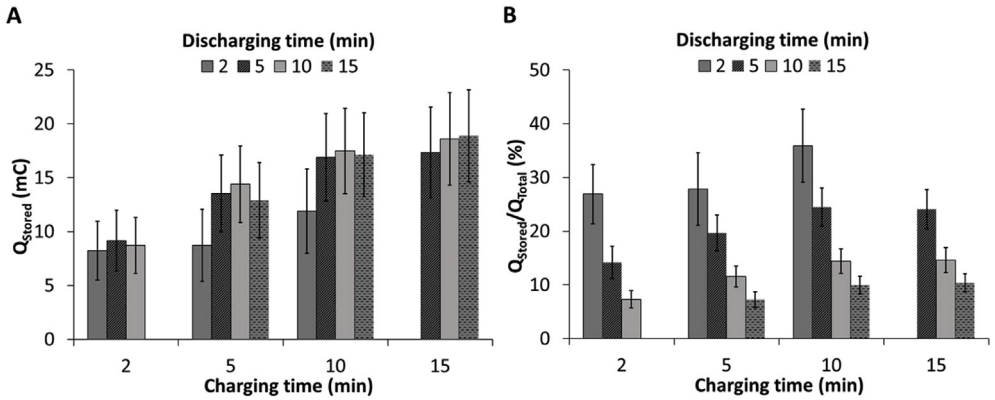

Fig. 6. A) Stored charge in absolute values (mC) for PK at −0.3 V vs Ag/AgCl. B) Stored charge contribution (%) to total produced charge for PK at −0.3 V vs Ag/AgCl. Combination of charging/discharging times were 2, 5, 10 and 15 min.

granules needs to be maximized, as it means larger surface area for bacterial growth will be available per unit of volume. The calculated SA:V ratio of the granules used in this study showed that larger granules have a lower ratio, which again indicated the preference towards the use of small AC granules.

If we look at charge storage normalized to granule volume, small GAC granules showed higher volumetric charge storage ($1.3 \pm 0.6\,mC\,L^{-1}$) than small PK granules ($0.74 \pm 0.3\,mC\,L^{-1}$) at -0.3 V discharging potential, even though the latter ones could store more charge per SSA. Once again, differences between the two type of granules were non-significant ($p = 0.1$). If we look at granule (PK) size, no linear relation could be found between charge storage and granule weight ($R^2 = 0.3$), current ($R^2 = 0.5$) or SSA ($R^2 = 0.3$). This could relate to an increased variability of charge storage with an increased granule size, as shown in the Supporting Information (chapter S6) as a function of SSA. Therefore, it is possible that other factors affect charge storage at increased granule size, such as larger potential drops, larger internal resistances due to ionic transport or lower actual SSA values, as previously measured on thick electrodes [60].

The specific capacitance of every granule was determined prior to bacterial inoculation. The average values obtained ranged from 4.9 to 6.1 $\mu F\,cm^{-2}$ for PK large, medium and small granules and 5 $\mu F\,cm^{-2}$ for small GAC granules (data not shown). These capacitance values differ several order of magnitudes from those measured (with aqueous electrolytes) for electrodes in MFCs (e.g. 13 10^{-3} $\mu F\,cm^{-2}$ for 3D-graphene nanosheets [18] or 0.5 10^{6} $\mu F\,cm^{-2}$ for carbon black [61]), but is more similar to electrodes measured in other research fields such as electrochemical double-layer capacitors (EDLCs) (e.g. 12.6 $\mu F\,cm^{-2}$ for activated carbon [35]) and capacitive deionization (CDI) (e.g. 12.2 $\mu F\,cm^{-2}$ for activated carbon cloth [59]). The measurement of electrode capacitance is complex and, when biofilm is present, difficult to determine as the faradaic current depends on the anode potential. Additionally, the open cell potential (OCP) of granules could not be determined with the MultiWE32 module. For these reasons, in this study charge storage instead of capacitance was reported, which describes the actual charge release by the capacitive bioanodes at a certain potential.

The studied charging/discharging time combinations are of importance when the capacitive properties of AC granules want to be optimally used. From the results we conclude that short charging and discharging times (2 min or less) are needed to achieve higher absolute values and larger contributions of stored charge compared to faradaic charge. Similarly, in terms of current output, short discharging times are preferred as the capacitive current is at highest. This is advantageous when using AC granules in fluidized MFC reactors, where often short discharging times are achieved. However, it is important to point out that, because of the constant movement of AC granules on fluidized bed reactors, electroactive biofilm might undergo a selective pressure in terms of e.g. biofilm thickness, microbial population and activity, that do not suffer under static conditions (this study). Particularly when the granules are in contact with each other and touch the current collector, the biofilm might get damaged and detached. Due to these shear forces, granules could erode and have a smoother surface, and bacteria might only grow in the inner mesopores in order to get protected from the outside, or could use more substrate for growth instead of for electricity production. Even though it is difficult to translate single granule performance to up-scaled reactors, this study can give valuable information about the potential of AC granules in MFCs: it shows the maximum performance such systems could achieve when conditions are ideal.

4. Conclusion

The study of single AC granules can lead to an optimized implementation of this kind of electrode material in up-scaled MFCs. The present study gives insight into the characterization of capacitive AC granules by means of electrochemical and microbiological analyses. Having a reactor with many granules is crucial for simultaneous and reproducible characterization of different types of granule properties, which similarly enables statistical analysis of results.

Acknowledgments

This research is supported by the Netherlands Organisation for Scientific Research (NWO), Domain Applied and Engineering Science (TTW) (VENI grant no 13631), and which is partly funded by the Ministry of Economic Affairs. The research was performed in cooperation with Wetsus, the European Centre of Excellence for Sustainable Water Technology. Wetsus is co-funded by the Dutch Ministry of Economic Affairs and Ministry of Infrastructure and Environment, the European Union Regional Development Fund, the Province of Fryslân, and the Northern Netherlands Provinces. The authors would like to thank the participants of the research theme “Resource Recovery” for the fruitful discussions and their financial support. Furthermore, the authors would like to thank Agnieszka Tomaszewska for helping with the SEM images.

Glossary

MCF	Microbial Fuel Cell
EAB	Electrochemically Active Bacteria
GAC	Granular Activated Carbon
SSA	Specific Surface Area
EDL	Electrochemical Double Layer
EDLC	Electrochemical Double-Layer Capacitor
TN	Total Nitrogen

Appendix A. Supplementary data

Supplementary data to this article can be found online at https://doi.org/10.1016/j.jpowsour.2019.04.042.

References

[1] B.E. Logan, B. Hamelers, R. Rozendal, U. Schoder, J. Keller, S. Freguia, P. Aelterman, W. Verstraete, K. Rabaey, Microbial fuel cells: methodology and technology, Environ. Sci. Technol. 40 (2006) 5181–5192, https://doi.org/10.1021/es0605016.
[2] B.E. Logan, J.M. Regan, Electricity-producing Bacterial Communities in Microbial Fuel Cells, (n.d.). doi:10.1016/j.tim.2006.10.003.
[3] T.H. Pham, K. Rabaey, P. Aelterman, P. Clauwaert, L. De Schamphelaire, N. Boon, W. Verstraete, Microbial fuel cells in relation to conventional anaerobic digestion technology, Eng. Life Sci. 6 (2006) 285–292, https://doi.org/10.1002/elsc.200620121.
[4] K. Rabaey, W. Verstraete, Microbial fuel cells: novel biotechnology for energy generation, Trends Biotechnol. 23 (2005) 291–298, https://doi.org/10.1016/j.tibtech.2005.04.008.
[5] T.H. Pham, P. Aelterman, W. Verstraete, Bioanode performance in bioelectrochemical systems: recent improvements and prospects, Trends Biotechnol. 27 (2009) 168–178, https://doi.org/10.1016/J.TIBTECH.2008.11.005.
[6] H. Liu, R. Ramnarayanan, B.E. Logan, Production of electricity during wastewater treatment using a single chamber microbial fuel cell, Environ. Sci. Technol. 38 (2004) 2281–2285, https://doi.org/10.1021/es034923g.
[7] K. Rabaey, R.A. Rozendal, Microbial electrosynthesis - revisiting the electrical route for microbial production, Nat. Rev. Microbiol. 8 (2010) 706–716, https://doi.org/10.1038/nrmicro2422.
[8] R. a. Rozendal, H.V.M. Hamelers, K. Rabaey, J. Keller, C.J.N. Buisman, Towards practical implementation of bioelectrochemical wastewater treatment, Trends Biotechnol. 26 (2008) 450–459, https://doi.org/10.1016/j.tibtech.2008.04.008.
[9] A. Deeke, T.H.J. a. Sleutels, T.F.W. Donkers, H.V.M. Hamelers, C.J.N. Buisman, A. Ter Heijne, Fluidized capacitive bioanode as a novel reactor concept for the microbial fuel cell, Environ. Sci. Technol. 49 (2015) 1929–1935, https://doi.org/10.1021/es503063n.
[10] A.P. Borole, C.Y. Hamilton, T. Vishnivetskaya, D. Leak, C. Andras, Improving power production in acetate-fed microbial fuel cells via enrichment of exoelectrogenic organisms in flow-through systems, Biochem. Eng. J. 48 (2009) 71–80, https://doi.org/10.1016/j.bej.2009.08.008.
[11] H. Wang, J. Do Park, Z. Ren, Active energy harvesting from microbial fuel cells at the maximum power point without using resistors, Environ. Sci. Technol. 46 (2012) 5247–5252, https://doi.org/10.1021/es300313d.
[12] B.E. Logan, M.J. Wallack, K.Y. Kim, W. He, Y. Feng, P.E. Saikaly, Assessment of microbial fuel cell configurations and power densities, Environ. Sci. Technol. Lett. 2 (2015) 206–214, https://doi.org/10.1021/acs.estlett.5b00180.

[13] S. Chen, S.A. Patil, R.K. Brown, U. Schröder, Strategies for optimizing the power output of microbial fuel cells: transitioning from fundamental studies to practical implementation, Appl. Energy 233–234 (2019) 15–28, https://doi.org/10.1016/j.apenergy.2018.10.015.
[14] C. Santoro, F. Soavi, A. Serov, C. Arbizzani, P. Atanassov, Self-powered supercapacitive microbial fuel cell: the ultimate way of boosting and harvesting power, Biosens. Bioelectron. 78 (2015) 229–235, https://doi.org/10.1016/j.bios.2015.11.026.
[15] J. Houghton, C. Santoro, F. Soavi, A. Serov, I. Ieropoulos, C. Arbizzani, P. Atanassov, Supercapacitive microbial fuel cell: characterization and analysis for improved charge storage/delivery performance, Bioresour. Technol. 218 (2016) 552–560, https://doi.org/10.1016/j.biortech.2016.06.105.
[16] A. Dewan, H. Beyenal, Z. Lewandowski, Intermittent energy harvesting improves the performance of microbial fuel cells, Environ. Sci. Technol. 43 (2009) 4600–4605, https://doi.org/10.1021/es8037092.
[17] C. Feng, Z. Lv, X. Yang, C. Wei, Anode modification with capacitive materials for a microbial fuel cell: an increase in transient power or stationary power, Phys. Chem. Chem. Phys. 16 (2014) 10464–10472, https://doi.org/10.1039/c4cp00923a.
[18] C. Santoro, M. Kodali, S. Kabir, F. Soavi, A. Serov, P. Atanassov, Three-dimensional graphene nanosheets as cathode catalysts in standard and supercapacitive microbial fuel cell, J. Power Sources 356 (2017) 371–380, https://doi.org/10.1016/j.jpowsour.2017.03.135.
[19] A. Deeke, T.H.J.A. Sleutels, H.V.M. Hamelers, C.J.N. Buisman, Capacitive bioanodes enable renewable energy storage in microbial fuel cells, Environ. Sci. Technol. 46 (2012) 3554–3560, https://doi.org/10.1021/es204126r.
[20] F. Li, Y. Sharma, Y. Lei, B. Li, Q. Zhou, Microbial fuel cells: the effects of configurations, electrolyte solutions, and electrode materials on power generation, Appl. Biochem. Biotechnol. 160 (2010) 168–181, https://doi.org/10.1007/s12010-008-8516-5.
[21] J. Hou, Z. Liu, P. Zhang, A new method for fabrication of graphene/polyaniline nanocomplex modified microbial fuel cell anodes, J. Power Sources 224 (2013) 139–144, https://doi.org/10.1016/J.JPOWSOUR.2012.09.091.
[22] J. Wei, P. Liang, X. Huang, Recent progress in electrodes for microbial fuel cells, Bioresour. Technol. 102 (2011) 9335–9344, https://doi.org/10.1016/j.biortech.2011.07.019.
[23] C. Santoro, C. Arbizzani, B. Erable, I. Ieropoulos, Microbial fuel cells: from fundamentals to applications. A review, J. Power Sources 356 (2017) 225–244, https://doi.org/10.1016/j.jpowsour.2017.03.109.
[24] H. Ren, S. Pyo, J.I. Lee, T.J. Park, F.S. Gittleson, F.C.C. Leung, J. Kim, A.D. Taylor, H.S. Lee, J. Chae, A high power density miniaturized microbial fuel cell having carbon nanotube anodes, J. Power Sources 273 (2015) 823–830, https://doi.org/10.1016/j.jpowsour.2014.09.165.
[25] P. Aelterman, M. Versichele, M. Marzorati, N. Boon, W. Verstraete, Loading rate and external resistance control the electricity generation of microbial fuel cells with different three-dimensional anodes, Bioresour. Technol. 99 (2008) 8895–8902, https://doi.org/10.1016/J.BIORTECH.2008.04.061.
[26] D. Qu, H. Shi, Studies of the activated carbons used in double-layer supercapacitors, J. Power Sources 74 (1998) 99–107, https://doi.org/10.1016/S0378-7753(02)00108-8.
[27] J. Wang, S. Kaskel, KOH activation of carbon-based materials for energy storage, J. Mater. Chem. 22 (2012) 23710–23725, https://doi.org/10.1039/c2jm34066f.
[28] E. Frackowiak, F. Béguin, Carbon materials for the electrochemical storage of energy in capacitors, Carbon N. Y. 39 (2001) 937–950, https://doi.org/10.1016/S0008-6223(00)00183-4.
[29] B. Kastening, M. Hahn, J. Kremeskötter, The double layer of activated carbon electrodes part 1. The contribution of ions in the pores, J. Electroanal. Chem. 374 (1994) 159–166, https://doi.org/10.1016/0022-0728(94)03373-0.
[30] M. Müllier, B. Kastening, The double layer of activated carbon electrodes, J. Electroanal. Chem. 374 (1994) 149–158, https://doi.org/10.1016/0022-0728(94)03372-2.
[31] L. Wei, G. Yushin, Electrical double layer capacitors with activated sucrose-derived carbon electrodes, Carbon N. Y. 49 (2011) 4830–4838, https://doi.org/10.1016/j.carbon.2011.07.003.
[32] P. Sharma, T.S. Bhatti, A review on electrochemical double-layer capacitors, Energy Convers. Manag. 51 (2010) 2901–2912, https://doi.org/10.1016/j.enconman.2010.06.031.
[33] Y. Zhang, H. Feng, X. Wu, L. Wang, A. Zhang, T. Xia, H. Dong, X. Li, L. Zhang, Progress of electrochemical capacitor electrode materials: a review, Int. J. Hydrogen Energy 34 (2009) 4889–4899, https://doi.org/10.1016/j.ijhydene.2009.04.005.
[34] C. Emmenegger, P. Mauron, P. Sudan, P. Wenger, V. Hermann, R. Gallay, A. Züttel, Investigation of electrochemical double-layer (ECDL) capacitors electrodes based on carbon nanotubes and activated carbon materials, J. Power Sources 124 (2003) 321–329, https://doi.org/10.1016/S0378-7753(03)00590-1.
[35] G. Gryglewicz, J. Machnikowski, E. Lorenc-Grabowska, G. Lota, E. Frackowiak, Effect of pore size distribution of coal-based activated carbons on double layer capacitance, Electrochim. Acta 50 (2005) 1197–1206, https://doi.org/10.1016/j.electacta.2004.07.045.
[36] A.G. Pandolfo, A.F. Hollenkamp, Carbon properties and their role in supercapacitors, J. Power Sources 157 (2006) 11–27, https://doi.org/10.1016/j.jpowsour.2006.02.065.
[37] W. Chen, Z. Liu, J. Hou, Y. Zhou, X. Lou, Y. Li, Enhancing performance of microbial fuel cells by using novel double-layer-capacitor-materials modified anodes, Int. J. Hydrogen Energy 43 (2018) 1816–1823, https://doi.org/10.1016/j.ijhydene.2017.11.034.
[38] X. Peng, H. Yu, X. Wang, Q. Zhou, S. Zhang, L. Geng, J. Sun, Z. Cai, Enhanced performance and capacitance behavior of anode by rolling Fe3O4 into activated carbon in microbial fuel cells, Bioresour, Technol. 121 (2012) 450–453, https://doi.org/10.1016/j.biortech.2012.06.021.
[39] J. Houghton, C. Santoro, F. Soavi, A. Serov, I. Ieropoulos, C. Arbizzani, P. Atanassov, Supercapacitive microbial fuel cell: characterization and analysis for improved charge storage/delivery performance, Bioresour. Technol. 218 (2016) 552–560, https://doi.org/10.1016/j.biortech.2016.06.105.
[40] J. Liu, F. Zhang, W. He, X. Zhang, Y. Feng, B.E. Logan, Intermittent contact of fluidized anode particles containing exoelectrogenic biofilms for continuous power generation in microbial fuel cells, J. Power Sources 261 (2014) 278–284, https://doi.org/10.1016/j.jpowsour.2014.03.071.
[41] S. Tejedor-Sanz, J.R. Quejigo, A. Berná, A. Esteve-Núñez, The planktonic relationship between fluid-like electrodes and bacteria: wiring in motion, ChemSusChem 10 (2017) 693–700, https://doi.org/10.1002/cssc.201601329.
[42] S. Tejedor-Sanz, J.M. Ortiz, A. Esteve-Núñez, Merging microbial electrochemical systems with electrocoagulation pretreatment for achieving a complete treatment of brewery wastewater, Chem. Eng. J. 330 (2017) 1068–1074, https://doi.org/10.1016/j.cej.2017.08.049.
[43] J. Liu, F. Zhang, W. He, W. Yang, Y. Feng, B.E. Logan, A microbial fluidized electrode electrolysis cell (MFEEC) for enhanced hydrogen production, J. Power Sources 271 (2014) 530–533, https://doi.org/10.1016/j.jpowsour.2014.08.042.
[44] J. Li, Z. Ge, Z. He, A fluidized bed membrane bioelectrochemical reactor for energy-efficient wastewater treatment, Bioresour. Technol. 167 (2014) 310–315, https://doi.org/10.1016/J.BIORTECH.2014.06.034.
[45] X. Wang, X. Yue, Q. Guo, Production of electricity during wastewater treatment using fluidized-bed microbial fuel cells, Chem. Eng. Technol. 37 (2014) 703–708, https://doi.org/10.1002/ceat.201300241.
[46] S. Tejedor-Sanz, P. Fernández-Labrador, S. Hart, C.I. Torres, A. Esteve-Núñez, Geobacter dominates the inner layers of a stratified biofilm on a fluidized anode during brewery wastewater treatment, Front. Microbiol. 9 (2018) 1–12, https://doi.org/10.3389/fmicb.2018.00378.
[47] T. Sleutels, S. Molenaar, A. Heijne, C. Buisman, Low substrate loading limits methanogenesis and leads to high coulombic efficiency in bioelectrochemical systems, Microorganisms 4 (2016) 1–11, https://doi.org/10.3390/microorganisms4010007.
[48] C. Borsje, D. Liu, T.H.J.A. Sleutels, C.J.N. Buisman, A. ter Heijne, Performance of single carbon granules as perspective for larger scale capacitive bioanodes, J. Power Sources 325 (2016) 690–696, https://doi.org/10.1016/j.jpowsour.2016.06.092.
[49] S. Wu, P. Liang, C. Zhang, H. Li, K. Zuo, X. Huang, Enhanced performance of microbial fuel cell at low substrate concentrations by adsorptive anode, Electrochim. Acta 161 (2015) 245–251, https://doi.org/10.1016/j.electacta.2015.02.028.
[50] S. Takahashi, J. Tomita, K. Nishioka, T. Hisada, M. Nishijima, Development of a prokaryotic universal primer for simultaneous analysis of Bacteria and Archaea using next-generation sequencing, PLoS One 9 (2014) e105592, , https://doi.org/10.1371/journal.pone.0105592.
[51] C. Quast, E. Pruesse, P. Yilmaz, J. Gerken, T. Schweer, P. Yarza, J. Peplies, F.O. Glöckner, The SILVA ribosomal RNA gene database project: improved data processing and web-based tools, Nucleic Acids Res. 41 (2013) 590–596, https://doi.org/10.1093/nar/gks1219.
[52] Q. Wang, G.M. Garrity, J.M. Tiedje, J.R. Cole, Naïve Bayesian classifier for rapid assignment of rRNA sequences into the new bacterial taxonomy, Appl. Environ. Microbiol. 73 (2007) 5261–5267, https://doi.org/10.1128/AEM.00062-07.
[53] S. Molenaar, T. Sleutels, J. Pereira, M. Lorio, C. Borsje, J.A. Zamudio, F. Fabregat-Santiago, C.J.N. Buisman, A. Heijne, In situ biofilm quantification in bioelectrochemical systems using optical coherence tomography, ChemSusChem 11 (2018) 1–9, https://doi.org/10.1002/cssc.201800589.
[54] D. Sun, J. Chen, H. Huang, W. Liu, Y. Ye, S. Cheng, The effect of biofilm thickness on electrochemical activity of Geobacter sulfurreducens, Int. J. Hydrogen Energy 41 (2016) 16523–16528, https://doi.org/10.1016/j.ijhydene.2016.04.163.
[55] D.R. Bond, D.R. Lovley, Electricity production by geobacter sulfurreducens attached to electrodes, Appl. Environ. Microbiol. 69 (2003) 1548–1555, https://doi.org/10.1128/AEM.69.3.1548.
[56] K. Guo, S. Freguia, P.G. Dennis, X. Chen, B.C. Donose, J. Keller, J.J. Gooding, K. Rabaey, Effects of surface charge and hydrophobicity on anodic biofilm formation, community composition, and current generation in bioelectrochemical systems, Environ. Sci. Technol. 47 (2013) 7563–7570, https://doi.org/10.1021/es400901u.
[57] C. Santoro, S. Babanova, K. Artyushkova, J.A. Cornejo, L. Ista, O. Bretschger, E. Marsili, P. Atanassov, A.J. Schuler, Influence of anode surface chemistry on microbial fuel cell operation, Bioelectrochemistry 106 (2015) 141–149, https://doi.org/10.1016/j.bioelechem.2015.05.002.
[58] X. Zhang, A. Prévoteau, R.O. Louro, C.M. Paquete, K. Rabaey, Periodic polarization of electroactive biofilms increases current density and charge carriers concentration while modifying biofilm structure, Biosens. Bioelectron. 121 (2018) 183–191, https://doi.org/10.1016/j.bios.2018.08.045.
[59] L. Han, K.G. Karthikeyan, M.A. Anderson, K.B. Gregory, Exploring the impact of pore size distribution on the performance of carbon electrodes for capacitive deionization, J. Colloid Interface Sci. 430 (2014) 93–99, https://doi.org/10.1016/j.jcis.2014.05.015.
[60] A. Deeke, T.H.J. a Sleutels, A. Ter Heijne, H.V.M. Hamelers, C.J.N. Buisman, Influence of the thickness of the capacitive layer on the performance of bioanodes in Microbial Fuel Cells, J. Power Sources 243 (2013) 611–616, https://doi.org/10.1016/j.jpowsour.2013.05.195.
[61] X. Peng, H. Yu, H. Yu, X. Wang, Lack of anodic capacitance causes power overshoot in microbial fuel cells, Bioresour. Technol. 138 (2013) 353–358, https://doi.org/10.1016/j.biortech.2013.03.187.